Određivanje potencijala geotermalnih ležišta s otopljenim ugljikovodičnim plinom

Determining the potential of geothermal reservoirs with dissolved hydrocarbon gas

dr. sc. Adaleta Perković
INA–Industrija nafte, d.d., Zagreb
adaleta.perkovic@ina.hr

dr. sc. Jasmina Jelić–Balta
INA–Industrija nafte, d.d., Zagreb
jasmina.jelic–balta@ina.hr

Maja Gregurić–Malekoci, dipl. ing.
INA–Industrija nafte, d.d., Zagreb
maja.greguric@ina.hr

Marko Gaćina, mag. ing.
INA–Industrija nafte, d.d., Zagreb
marko.gacina@ina.hr

Ključne riječi: ugljikovodični plin, geotermalna energija, ležišna simulacija, Monte Carlo metoda

Key words: Hydrocarbon gas, geothermal energy, reservoir simulation, Monte Carlo method

Sažetak

S obzirom da je rast i razvoj geotermalne energije usko povezan i s naftnom industrijom, u radu je evaluirana mogućnost iskorištavanja geotermalnih ležišta gdje osim vode, u ležištu postoji i određena količina otopljenog plina koji u svom sastavu sadrži i ugljikovodike. Uloga takvog plina mogla bi biti značajna u podizanju rentabilnosti razvoja geotermalnog projekta, posebno u njegovom začetku.

Glavni cilj rada je dati potrebne tehničke parametre kako bi se mogla izvršiti tehno-ekonomska analiza geotermalnog projekta koji se koristi već izbušenim bušotinama, rađenim za potrebe istraživanja ugljikovodika. U radu su korišteni seizmički podaci uz pomoć kojih je određena površina ležišta, bušotinski (karotažni) podaci za određivanje pojedinih litologija i debljina slojeva te njihove poroznosti. Također, korištena su i DST ispitivanja iz kojih je potvrđeno da su određeni slojevi zasićeni osim vode i s plinom u kojem udio ugljičnog dioksida i ugljikovodičnih komponenti varira ovisno o ispitivanom sloju.

Obzirom da se radi o plinu otopljenom u vodi, potrebno je bilo upotrebom ležišne simulacije odrediti njegov iscrpak pri simultanoj proizvodnji plinom zasićene vode te utiskivanju degazirane. Provedeni su različiti simulacijski slučajevi koji pokrivaju MIN, MAX i MED petrofizikalne setove podataka te su uspoređeni s rezultatima prethodno kreiranog Monte Carlo modela. Osim ukupnog iscrpka plina, razmatrano je i ponašanje ležišnog tlaka i temperature u projektnom razdoblju od 30 godina.

Abstract

Since development and growth of geothermal energy is closely related to oil industry, in this paper we evaluate the possibility of geothermal reservoir production in which, in addition to water, a reservoir contains

dissolved gas composed mostly of methane and carbon dioxide. Such gas could increase the cost-effectiveness of the development of a geothermal project, especially in its beginnings.

The main focus of this work is to provide the required technical parameters such that a techno-economic analysis could be made for the cost-effectiveness of a geothermal project which utilizes pre-existing boreholes, made initially for hydrocarbon exploration. The study utilizes seismic data which was used to determine the reservoir area, well log data for the assessment of various lithologies, layer thicknesses and their porosities. Furthermore, DST analyses were observed from which can be seen that specific layers were saturated with water and gas and the proportion of carbon dioxide and hydrocarbon components varies according to reservoir depth.

Since we are dealing with the gas originally dissolved in water, it was necessary to create a reservoir simulation model in order to determine its recovery factor while simultaneously producing gas saturated water and injecting degassed water. Different simulation cases were carried out, covering MIN, MAX and MED petrophysical datasets and are compared to the results of the previously created Monte Carlo model. In addition to the total gas recovery, we also considered the behavior of the reservoir pressure and temperature in a project lifetime of 30 years.

Table 1. Available reservoir data obtained from DST well testing.

DST–1		DST–4	
Section (m)	3388.8 – 3407	Section (m)	4191.43 – 4198
T (°C)	153.15	T (°C)	183
p (bar)	489.19	p (bar)	390.336
lithology	fractured marl	lithology	fractured dolomite
fluids produced	oil	fluids produced	brine, gas
productivity	low	productivity	good permeability, high skin
DST–2		DST–5	
Section (m)	3452.5 – 3470	Section (m)	3403–3413
T (°C)	185	T (°C)	173
p (bar)	489.19	p (bar)	422
lithology	–	lithology	fractured dolomite
fluids produced	NA	fluids produced	oil
productivity	low	productivity	low
DST–3			
Section (m)	3924 – 3963		
T (°C)	191.5		
p (bar)	380		
lithology	silty quartz sandstone		
fluids produced	gas		
productivity	boundary conditions reached		

1. Introduction

Besides water, deeper geothermal reservoirs always contain some amount of dissolved gas. Usually, the gas composition is mostly carbon dioxide but sometimes it is enriched with lighter hydrocarbons, namely methane. Those hydrocarbons could potentially be of a great interest if their amount is significant which is mostly related to the pressure and temperature conditions in the reservoir and water production rates.

In this work, we have considered a potential geothermal reservoir located in the Croatian part of the Pannonian basin for which data collected during a well DST performance was available as well as petrophysical data, gas and water analyses and geological and seismic studies. The prospect was explored during the 1980s in order to find oil and gas reserves. Data collected served for the initialization of the conceptual reservoir simulation models.

Considering very high investment needs at the beginning of every geothermal project, namely drilling wells and building the power plant, additional income coming from the hydrocarbon gas could have a key role in project economics and investment return rate.

1.1. Well history

Up to now, all of the previously drilled wells have been abandoned except a well which targeted formations more than 5000 m deep. During the drilling part and short well testing, the well did not provide any feasible quantities of hydrocarbons. The interval tested around 3500 m located in a basalt formation produced small amounts of light oil while deeper parts, up to 4165 m, located in breccia and conglomerate rock type formations, produced light gas and water. The most interesting fact is that during the

Table 2. Gas compositions according to the depth of the reservoir.

Depth (m)	3924–3963	3924–3963	4191–4198	4191–4198	4054–4077	4054–4077
Composition	vol%	vol%	vol%	vol%	vol%	vol%
CO_2	0.65	0.75	49.41	56.58	17.05	13.89
N_2	0.99	2.26	2.43	5.80	–	2.23
C_1	74.65	73.63	44.20	36.97	67.99	64.96
C_2	12.77	12.56	1.46	0.53	8.90	9.39
C_3	4.89	4.80	1.55	0.04	3.54	4.61
$i\text{-}C_4$	2.14	2.04	0.21	0.01	0.75	1.04
$n\text{-}C_4$	1.52	1.35	0.44	0.02	1.02	1.81
$i\text{-}C_5$	0.81	0.80	0.07	0.01	0.26	0.61
$n\text{-}C_5$	0.31	0.30	0.09	–	0.20	0.52
C_{6+}	1.27	1.45	0.09	–	0.24	0.89

drilling at depths near 4200 m, all drilling fluid was lost, indicating very favorable reservoir properties. The formation rock at the tested depth is naturally fractured dolomite which has a thickness of more than 400 m, up to nearly 4600 m of measured depth (MD), where the breccia type of rock starts and it lasts up to at least the well's total depth of 5051 m MD. **Table 1** lists the most relevant data obtained from DST well testing.

In order to quantify the productivity of the naturally fractured zone and to prove the presence of hydrocarbon gas, a section from 4191 up to 4198 m was tested. During the test, formation brine along with some quantities of gas was produced. The results showed severe formation damage due to drilling mud filtrate resulting in an average water rate of 165.65 m^3/day and calculated permeability of 399.8 mD. The reported formation temperature at 4198 m is 182°C while the pressure was around 390 bar. Two gas samples were collected and analyzed during the DST, reporting the methane content of 36.97 and 44.20 vol%. A list of reported gas compositions originating from all deeper sections is given in Table 2.

The formation temperature, along with the naturally fractured dolomite, its thickness and high conductivity, point to a reservoir of good geothermal potential with a possible economically significant amount of dissolved gas containing mostly carbon dioxide and methane.

Since the reservoir data is missing some key information from the well testing, conceptual numerical models are created in order to study the production of dissolved gas in a 30 year lifespan.

2. Monte Carlo model

For this project a simple Monte Carlo model was first created as part of an exploration study, in order to make a prediction about the possible power plant's installed capacity utilizing the production of hot water. A similar approach was presented by **Barylo (2000)**, and **Ofwona (2014)**. The input data for the Monte Carlo simulation is given in **Table 3** and the results are given in **Figure 1**. As can be seen from the results, there is a 50% probability of achieving 13.3 MW power capacity, 90% for 9 MW and 10% to achieve 18.5 MW. The model consists of a total of 5000 iterations that calculate the available reservoir energy and then the potential power capacity, according to **Equation 1**.

$$MWe = \frac{Available\ energy \times Recovery\ factor \times Efficiency\ factor}{Load\ factor \times Life\ time}$$

Most of the total available energy in the reservoir is stored as heat within the rocks whereas the fluids contain only a small portion. Available energy can be calculated from **Equation 2**.

$$E_{total} = V\,\rho_r c_r (1-\Phi)(T - T_{ref}) + V\,\rho_f c_f\,\Phi\,(T - T_{ref})$$

Where: – total available energy (J), – reservoir volume (m^3), – rock density (kg/m^3), – rock specific heat (J/kg°C), – rock porosity (fraction), – reservoir initial temperature (°C), – reservoir reference temperature (°C), – fluid density (kg/m^3), – fluid specific heat (J/kg°C)

Table 3. Monte Carlo method input data.

Parameter	Min	Med	Max	Distribution
Area (km^2)	26	28	30	square
Reservoir thickness (m)	200	400	700	triangle
Rock density (kg/m^3)	2700	2700	2700	const
Rock specific heat (J/kg°C)	1000	1000	1000	const
Porosity, fraction	0.02	0.04	0.06	triangle
Reservoir temperature (°C)	180	185	200	triangle
Reference temperature (°C)	140	140	140	const
Fluid density (kg/m^3)	858.77	881.61	887.01	steam tables
Fluid specific heat (J/kg°C)	4406	4425	4494	steam tables

Parameter	Min	Med	Max	Distribution
Recovery factor	0.025	0.05	0.075	triangle
Conversion efficiency	0.12	0.12	0.12	const
Plant life – 25 years (s)	7.884E +08	7.884E +08	7.884E +08	const
Load factor	0.9	0.9	0.9	const
h_{final}@140°C (J/kg)	589200	589200	589200	Const

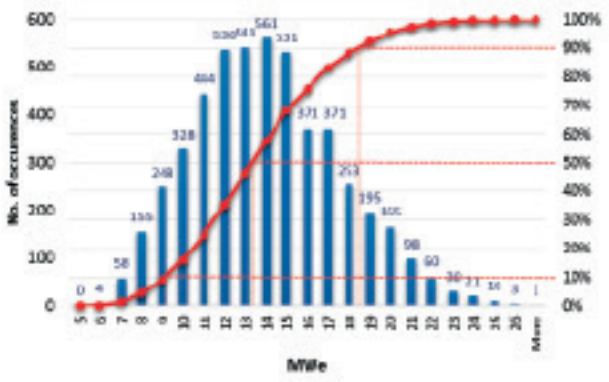

Figure 1. The results of a Monte Carlo model.

An estimation of the recovery factor (Rf) is always a tricky task, especially when no core data is available for the range of interest. Various numbers are reported by different authors and one of the recent estimations made by Grant (2015) is to use a recovery factor of 10%. In our case, a more conservative approach was used for the Monte Carlo model, where the value for the recovery factor was varied from 2.5 to 7.5% and the reference temperature was set to 140°C for the observed period of time of 25 years.

Although this approach can shed more light onto the geothermal potential of the prospect, there is still no insight at the geothermal water rate production estimation nor gas production and recovery factor. For that reason, it was decided to perform the conceptual numerical modeling in order to get a more detailed estimation of the heat and gas recovery factors.

3. Numerical simulation

Simulation models were built in Schlumberger Eclipse numerical modeling software as a compositional models consisting of 3 components – water (with 10,000 ppm of dissolved sodium chloride), carbon dioxide and methane. In order to quantify the effect of key properties, sensitivity analysis was performed and different simulation cases created by altering water and gas reserves (altering reservoir thickness), permeability, gas compositions and distance between wells.

Two groups of fluid compositions were used – one with water concentration of 99.2 mol% giving an overall gas-water ratio (GWR) of around 9 m^3, and a second one with 99.7 mol% water concentration, resulting in a GWR of around 3 m^3. Base case model properties are given in Table 4 while detailed reservoir fluid compositions, corresponding saturation pressures, GWR and heating values are given in Table 5.

3.1. Base case model

Generally, the base case model consists of a total of 25,000 active grid cells (50 × 50 × 10) with grid blocks spacing of 106 × 106 m and reservoir thickness of 100 m (**Figure 2**). Porosity and permeability values were set uniformly for the whole reservoir, 6% and 100 mD respectively. The model is initially 100% water saturated with GWR of 8.9 m^3/m^3. Prediction scenarios include doublet system. Distance between the producer and injector is set to 1900 m in order to avoid the cold front short cutting to the producer well. Reservoir temperature is 185°C and reservoir pressure is set to 400 bar, while the reservoir brine saturation pressure is at 383.7 bar, keeping all the gas dissolved in water. Injection stream is degassed water with injection rate of 10,000 m^3/d (around 115 l/s). The production is governed by the constant water rate control of 10,000 m^3/d. The same production constraints were used in other simulation cases. Produced gas is not injected back in the reservoir which results in a slight pressure decrease over an observed project lifetime of 30 years (Figure 9).

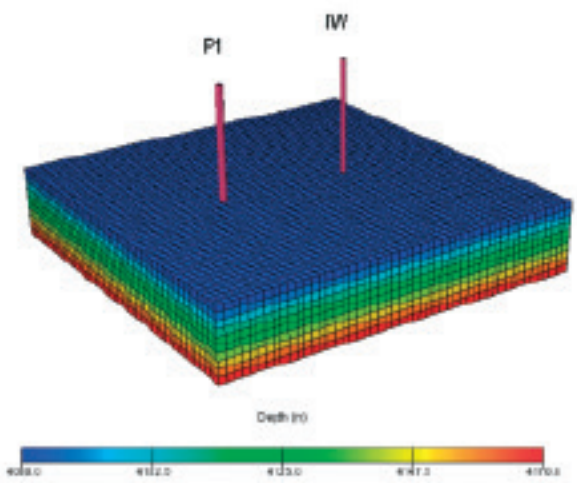

Figure 2. 3D view of simulation model (Depth, m)

Table 4. Base case simulation model properties.

Base case model properties	
Grid dimensions	50 x 50 x 10
Total Active grid blocks	25000
Gridblock spacing (m)	106
Thickness (m)	100
Top layer depth (m)	4075
Area (km^2)	28.09
Permeability (mD)	100
Porosity	0.06
Initial pressure (bar)	400
Initial temperature (°C)	185
Reservoir volume of water (10^6 Rm^3)	168.571
Total volume of gas dissolved in water (10^6 Sm^3)	1295.210
Reservoir fluid composition (mol%)	
CO_2	0.272
H_2O	99.200
C_1	0.528
Thermal properties	
Temperature of injected water, °C	30
Thermal conductivity of rock, $Wm^{-1}K^{-1}$	4
Water phase thermal conductivity, $Wm^{-1}K^{-1}$	0.6
Rock heat capacity, $Jkg^{-1}K^{-1}$	1000
Well	
Perforations	through the whole reservoir
Distance between producer – injector (m)	1900

3.2. Reservoir fluid model

Since a simulation model uses an equation of state (EOS) to calculate reservoir fluid properties, a ternary fluid model consisting of H_2O, CO_2 and C_1 was built in IPM PTVp software adding just binary interaction parameters (BIP) for all the component pairs, presented in **Table 6**. BIP for the C_1-H_2O pair was taken according to **Ganjdanesh and Hosseini (2016),** where the CO_2-C_1 and CO_2-H_2O BIP were obtained from **Li and Yang (2013)**. During the well testing, GWR value was not measured, hence the assumption was that the maximum amount of gas is dissolved in the water what is nearly 9 sm^3/sm^3 at reservoir conditions, obtained by the Peng Robinson equation of state (PR EOS), **Peng and Robinson (1976)**. Looking at **Figure 3**, a descending trend can be observed in saturation pressure (Psat) and gas-water ratio (GWR), with increasing CO_2 content. Different researchers observed that adding CO_2 in CO_2 – hydrocarbon gas mixtures result in a higher overall mixture solubility in water, **Blount et al (1982)**. In a CO_2-C_1 mixture, looking only at the methane solubility, adding a small amounts of CO_2 increases its solubility after which the methane is pushed out of a solution by further CO_2 addition. Concerning the GWR, authors suggest that different types of reservoir fluids exist, where one group's saturation pressure is close to the reservoir pressure and the other type which is largely undersaturated. In this work, we have also considered both reservoir fluid types, named group 1 and group 2.

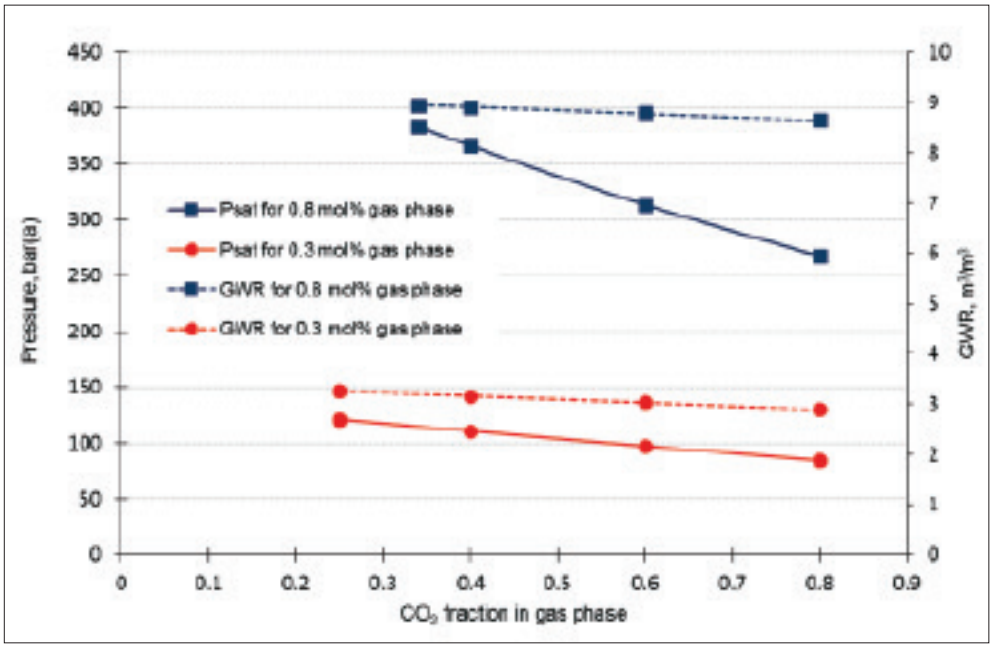

Figure 3. Behavior of the saturation pressure, Psat and GWR as a function of pressure and CO_2 content.

Table 5. Reservoir fluid and resulting gas phase compositions used throughout the work.

GROUP 1 – GWR ~ 9 m^3/m^3			GROUP 2 – GWR ~ 3 m^3/m^3		
	Reservoir fluid composition (mol%)	Gas composition (mol%)		Reservoir fluid composition (mol%)	Gas composition (mol%)
H_2O	99.200		H_2O	99.700	
CO_2	0.272	0.340	CO_2	0.075	0.250
C_1	0.528	0.660	C_1	0.225	0.750
Lower gas cal. value (MJ/m^3)		22.473	Lower gas cal. value (MJ/m^3)		22.473
Psat (bara)		383.70	Psat (bara)		121.09
GWR (m^3/m^3)		8.954	GWR (m^3/m^3)		3.257
H_2O	99.20		H_2O	99.700	
CO_2	0.320	0.400	CO_2	0.120	0.400
C_1	0.480	0.600	C_1	0.180	0.600
Lower gas cal. value (MJ/m^3)		20.435	Lower gas cal. value (MJ/m^3)		20.435
Psat (bara)		366.26	Psat (bara)		110.75
GWR (m^3/m^3)		8.914	GWR (m^3/m^3)		3.165
H_2O	99.200		H_2O	99.700	
CO_2	0.480	0.600	CO_2	0.180	0.600
C_1	0.320	0.400	C_1	0.120	0.400
Lower gas cal. value (MJ/m^3)		13.633	Lower gas cal. value (MJ/m^3)		13.633
Psat (bara)		313.41	Psat (bara)		97.47
GWR (m^3/m^3)		8.781	GWR (m^3/m^3)		3.035
H_2O	99.200		H_2O	99.700	
CO_2	0.640	0.800	CO_2	0.240	0.800
C_1	0.160	0.200	C_1	0.060	0.200
Lower gas cal. value (MJ/m^3)		6.822	Lower gas cal. value (MJ/m^3)		6.822
Psat (bara)		267.71	Psat (bara)		84.75
GWR (m^3/m^3)		8.643	GWR (m^3/m^3)		2.893

Table 6. Binary interaction parameters used for reservoir fluid modeling.

	H_2O	CO_2	C_1
H_2O	–		
CO_2	0.1896	–	
C_1	0.056	0.13	–

3.3. Temperature effects

Since the temperature of produced water controls the available energy at the surface, it is necessary to predict the time when the temperature of produced fluid starts to decrease. To check for temperature changes in a reservoir, different cases were simulated by varying the reservoir permeability and well spacing. The water injection temperature is set to 30°C. Due to the simulator limitations, only these temperature dependent models were created as black oil type.

Permeability is set to 100 mD in the base case, where in other cases to 50 and 400 mD, respectively. Higher reservoir permeability enables a cold front to reach the producer sooner. In most unfavorable model with the 50 mD permeability, the front reaches the producer after more than 90 years of constant water production and injection rate of 10,000 m^3/day (**Figure 4**). While lower permeability is favorable for the delay of temperature decrease, and although there were negligible differences in gas production, there was significant increase in differential pressures for both the injection and production. As expected, the distance between wells delays temperature drop at the production well (with 1900 m distance after 60 years, **Figure 5** and **6**).

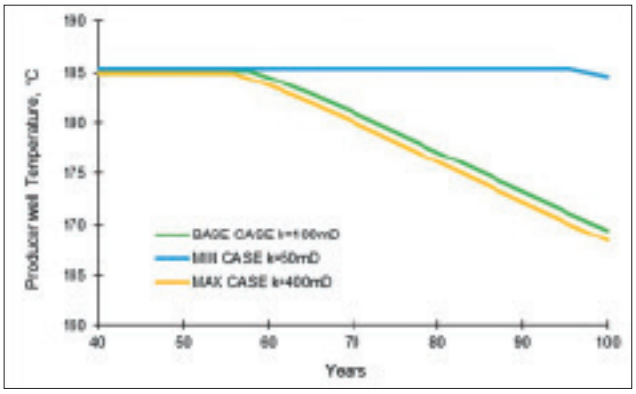

Figure 4. Reservoir temperature in respect to different reservoir permeabilities.

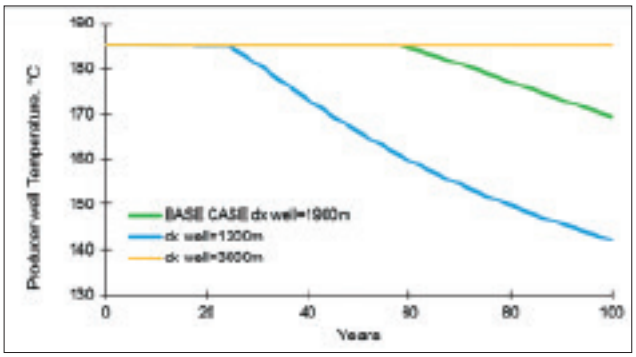

Figure 5. Reservoir temperature in respect to different well distances.

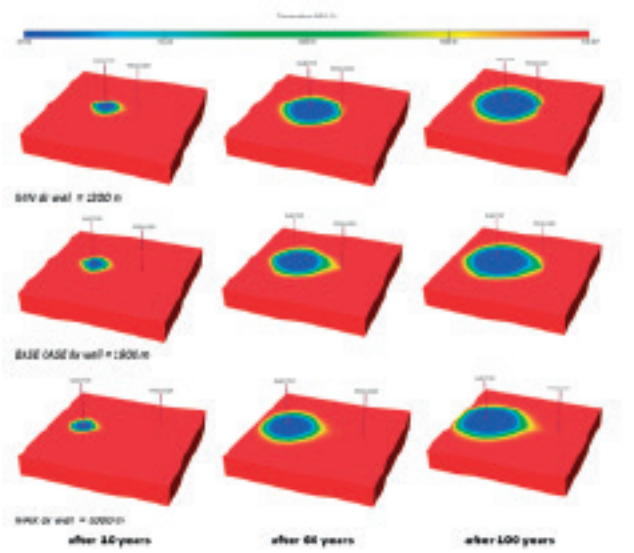

Figure 6. Temperature distribution in the reservoir for different producer–injector well distances

3.4. Simulation cases concerning the gas production

3.4.1. Reserves variation

Based on MMRA analyses, available water reserves were altered by changing the overall reservoir thickness from 20 to 400 m compared to the base case model (100 m). Reservoir volumes of water and surface gas volumes are given in **Table 7** for inspected cases. The goal was to see the effect on the gas production and ultimate recovery. For all the cases, production prediction is given for a 30 year period. Results are showing the gas production plateau (around 90,000 m^3/d) for a 12 year period in the maximum reserves case with a gas recovery of around 20%. Base case has around 3.5 years of production plateau, and final gas recovery of 40%. Case utilizing the minimum reserves reaches the gas rate economic limit of 10,000 m^3/d after 15 years with the highest recovery factor. The results are given graphically in Figure 7 and Table 7.

Composition of produced gas for a base case was also inspected in respect to different reserves values as shown in Figure 8 while reservoir pressure behavior through project lifetime can be seen in Figure 9. It is evident that due to a higher methane reservoir mobility compared to CO_2 when the reservoir pressure drops below the saturation pressure, overall

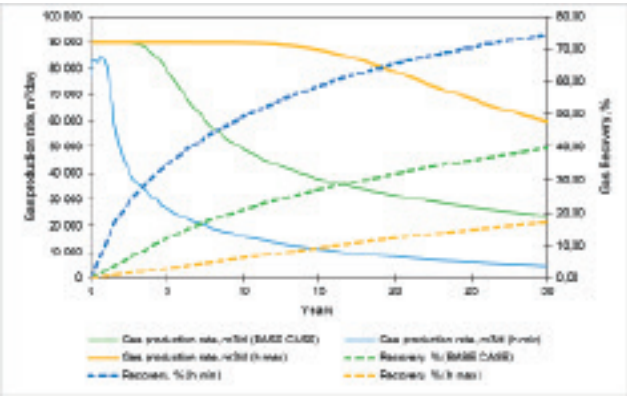

Figure 7. Gas production rates and final recovery for different gas reserves estimation

Table 7. Gas recoveries for different water and gas reserves cases

Case	Reservoir Volume of Water	Total Gas dissolved in water (surface volume)	Surface volume of water	Gas production Total	Gas Recovery
	10^6 Rm^3	10^6 Sm^3	10^6 Sm^3	10^6 Sm^3	%
BASE CASE	168.571	1,295.210	144.326	513	39.58
GAS_DISSOLV_MIN	33.709	258.965	28.857	193	74.33
GAS_DISSOLV_MAX	674.657	5,186.623	577.950	892	17.20

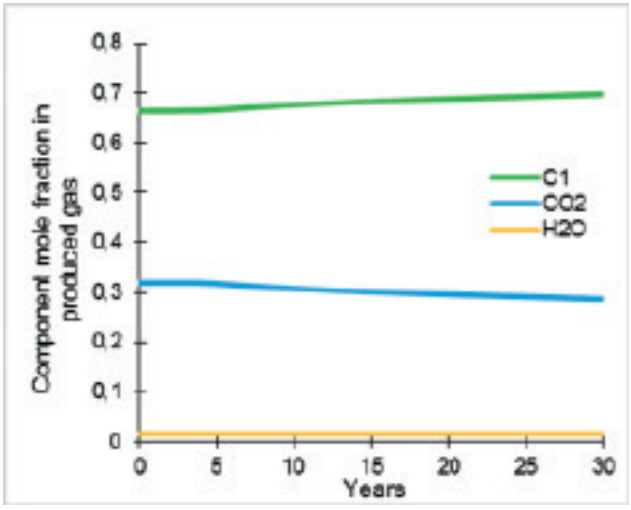

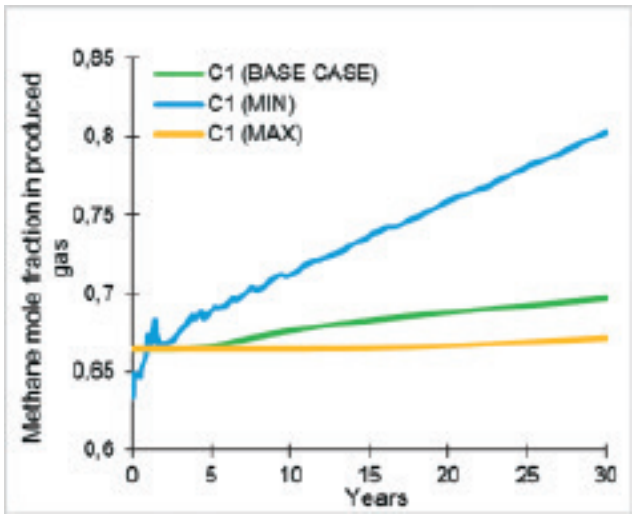

Figure 8. Base case component mole fractions in gas produced (left) and methane mole fraction in produced gas for different gas reserves estimations (right)

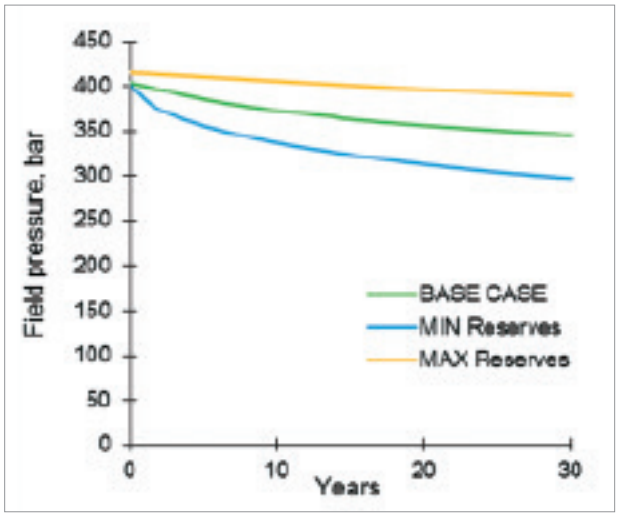

Figure 9. Prediction of field pressure for different reserves estimations

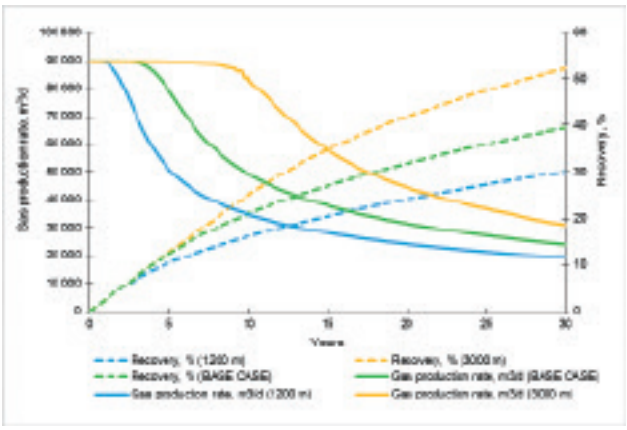

Figure 10. Gas production rates and final recovery for different well spacing cases

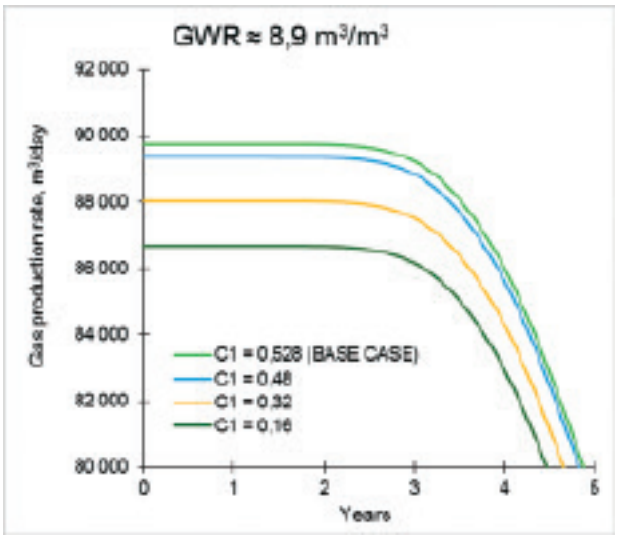

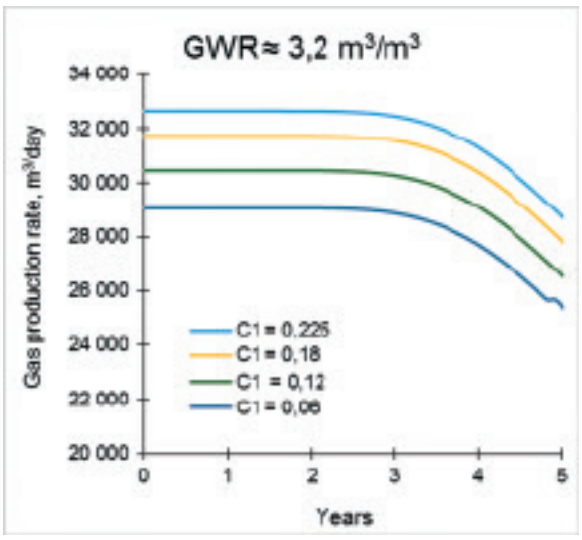

Figure 11. Gas production rate due to different methane content in dissolved gas.

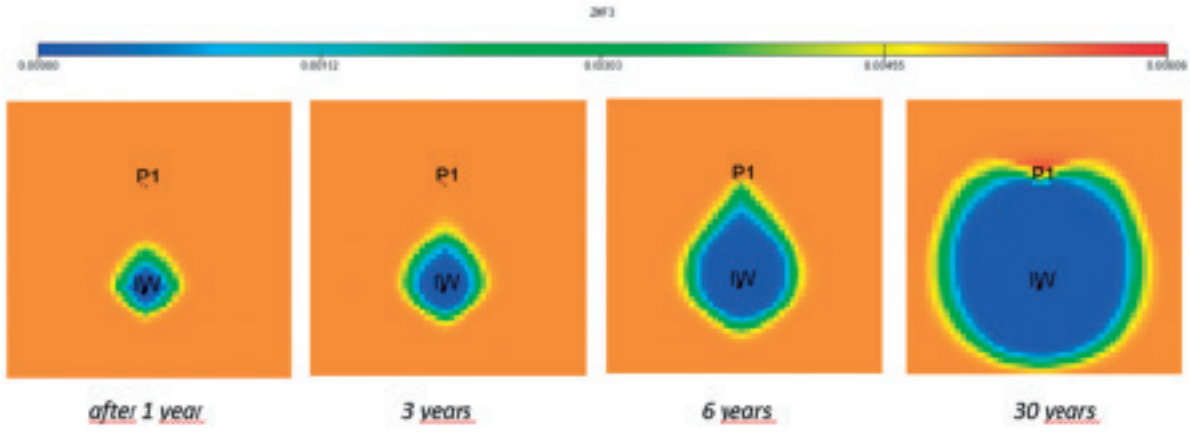

Figure 12. Prediction of methane mole fraction in dissolved gas (base case)

methane production and recovery is higher, especially in the case of minimal gas reserves (minimal reservoir thickness).

3.4.2. Well spacing

Two different cases were performed besides the base case, with well distances as in temperature models, 1200 and 3000 m. In the base case (1900 m) gas production plateau is around 3.5 years and as distance between the wells increase, production plateau also extends (**Figure 10**).

3.4.3. Gas composition

To observe the impact of different gas compositions in terms of carbon dioxide and methane proportions, fluids with the compositions from **Table 5** were used. Although slightly higher from the fractured dolomite formation, at the depths around 4060 m, the measured and reported methane content in the gas composition is 64.96 mol%, it is more probable that the methane content is getting lower in respect to depth. The results of compositional variations are shown in **Figure 11** and **12**.

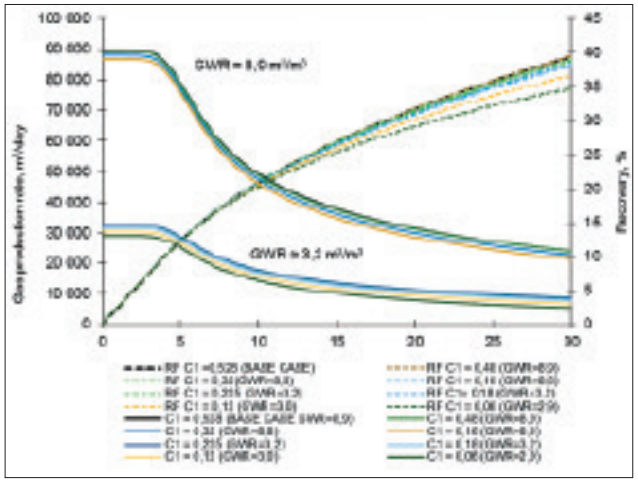

Figure 13. Gas production rates and final recoveries for composition variations

Larger methane content in dissolved gas affects the gas production by slightly increasing the GWR (**Figure 10**). It is indicated also in a little bit higher recoveries (**Figure 12**). For all simulated base case composition variations, gas recoveries are in the range of 35 to 40%.

4. Energy potential comparison

The goal of this work was to observe the gas production potential and gas recovery factor in order to estimate its energy contribution compared to the energy coming from hot water production. In this section, simple energy and power related calculations are presented where the complex surface processes and equipment are not considered and are beyond the scope of this work. To estimate the power potential by hot water production, an approach described by **Dickson and Fanelli (2013)** was used and applied to a base case scenario which does not differ largely from other cases, observing only water production. **Equations 3** and **4** for calculating the net generated electric power (NEP) by available thermal power (ATP) are used and **Table 7** lists all the input data and obtained results. Water temperature at power plant inlet is assumed to be 160°C (438 K), and the pressure used was 20 bar(a), resulting in a density of 908.27 kg/m^3 which is the value used for mass flow calculation. Power plant outlet water temperature is assumed to be 75°C (348 K).

In order to calculate the potential power coming from the gas source, lower heating values are calculated.

All the input data and obtained results for the base case model with various gas compositions are given in Table 8. Different gas rates are considered related to different gas compositions and amount of gas dissolved. It is crucial to understand that the reported electric power is available for only a fraction of time, depending on total reserves, well distance, etc. The plateau of maximum gas production can be observed e.g. in Figure 9, yielding production time period of a minimum of 1 year up to 3.5 and 10 years in respect to different well spacing. After that time, gas production rates constantly decrease over time.

$$NEP = \frac{(0.18 \times T_{in} - 10) \times ATP}{278}$$

Where: – net electric power (kW), – water temperature at the power plant inlet (K), – available thermal power (kW).

ATP is calculated from:

$$ATP = \dot{m} \times c_p \times (T_{in-} T_{out})$$

Where: – mass flow (kg/s), – specific heat capacity of water (kJ/kgK), – water temperature at the power plant inlet (K), – water temperature at the power plant outlet (K).

5. Conclusion

The results for the power potential of geothermal water obtained by the Monte Carlo method and the one obtained by numerical modeling coupled with simple power related calculations are in good agreement and of the same order of magnitude. On the other hand, it is impossible to predict the impact of a dissolved gas using Monte Carlo approach which is why we suggest using reservoir simulation models instead.

Gas production from created models indicates potentially significant quantities, especially at the very beginning, when the GWR is constant. It is clear that in order to keep the gas production plateau constant for a longer period of time, well spacing and overall reserves in place are important. The models also confirmed that the front of a gas free water is advancing far more rapidly compared to a cold water front. Ultimate gas recoveries could be quite high suggesting a further, more complex investigation is preferred (e.g. building full-field geological model).

Table 7. Water related power estimation

Q_w (m^3/day)	r_w, (kg/m^3)	c_p (kJ/kgK)	T_{in} (K)	T_{out} (K)	m (kg/s)	ATP (MW)	NEP (MWe)
10,000	908.27	4.33	438	348	105.12	40.97	**10.14**

Table 8. Gas related maximum power estimation

Q_g (m^3/day)	C_1 (mol%)	Lower heating value, (MJ/m^3)	Stream power (MJ/day)	Stream power (MW)	Conversion efficiency	Power (MWe)
89,540	0.66	22.47	2,012,277	23.29	0.5	**11.65**
89,140	0.60	20.43	1,821,539	21.08	0.5	**10.54**
87,810	0.40	13.63	1,197,105	13.86	0.5	**6.93**
86,430	0.20	6.82	589,614	6.82	0.5	**3.41**
32,570	0.75	25.53	831,533	9.62	0.5	**4.81**
31,650	0.60	20.43	646,755	7.49	0.5	**3.74**
30,350	0.40	13.63	413,758	4.79	0.5	**2.39**
28,930	0.20	6.82	197,357	2.28	0.5	**1.14**

One of the next steps in investigating the benefits of the production of initially dissolved gas would be to consider the possible gas utilization scheme covering all technical (surface processes and equipment), financial and legislation aspects for the calculation of net energy balance and cost benefit analysis.

Concerning future work, in order to perform more accurate fluid models of dissolved gas in water, it would be beneficial to experimentally investigate the solubility of different gas compositions and thus obtain the right BIP values. If the accuracy is not of a concern, e.g. performing only conceptual models and hence there is no large difference between the different compositions used in terms of a overall gas production, it would be possible to obtain similar results by using simpler black oil models. In terms of the accuracy of the simulation models, production data from the well testing is crucial as well as the right geological and petrophysical information. In situations when dealing with the fractured reservoirs, it would be wise to create dual porosity model if required data is available.

Literatura

1. Barylo, A. (2000). *Assessment of the energy potential of the Beregovsky geothermal system, Ukraine*. United Nations University.
2. Blount, C. W., & Price, L. C. (1982). *Solubility of Methane in Water Under Natural Conditions: A Laboratory Study. Final Report, DOE Contract No*. DE-A508-78ET12145.
3. Dickson, M. H., & Fanelli, M. (2013). *Geothermal energy: utilization and technology*. Routledge.
4. DiPippo, R. (Ed.). (2016). *Geothermal power generation: Developments and innovation*. Woodhead Publishing.
5. Duan, Z., & Mao, S. (2006). A thermodynamic model for calculating methane solubility, density and gas phase composition of methane-bearing aqueous fluids from 273 to 523 K and from 1 to 2000 bar. *Geochimica et Cosmochimica Acta*, 70(13), 3369-3386.
6. Ganjdanesh, R., & Hosseini, S. A. (2016). Potential assessment of methane and heat production from geopressured–geothermal aquifers. *Geothermal Energy*, 4(1), 16.
7. Grant, M. A. (2015). Resource assessment, a review, with reference to the Australian code. *Resource*, *19*, 25
8. Li, X., & Yang, D. (2013). Determination of Mutual Solubility between CO_2 and Water by Using the Peng–Robinson Equation of State with Modified Alpha Function and Binary Interaction Parameter. *Industrial & Engineering Chemistry Research*, 52(38), 13829-13838.
9. Mao, S., Hu, J., Zhang, D., & Li, Y. (2013). Thermodynamic modeling of ternary $CH4H_2ONaCl$ fluid inclusions. *Chemical Geology*, *335*, 128–135.
10. Ofwona, C. O. (2014). Geothermal resource assessment: case example, Olkaria I. *001374011*.
11. Peng, D. Y., & Robinson, D. B. (1976). A new two-constant equation of state. *Industrial & Engineering Chemistry Fundamentals*, 15(1), 59-64.
12. Trota, A., Ferreira, P., Gomes, L., Cabral, J., & Kallberg, P. (2019). Power Production Estimates from Geothermal Resources by Means of Small-Size Compact Climeon Heat Power Converters: Case Studies from Portugal (Sete Cidades, Azores and Longroiva Spa, Mainland). *Energies*, 12(14), 2838.
13. Ziabakhsh-Ganji, Z., & Kooi, H. (2012). An Equation of State for thermodynamic equilibrium of gas mixtures and brines to allow simulation of the effects of impurities in subsurface CO_2 storage. *International Journal of Greenhouse Gas Control*, *11*, S21-S34.